Renormalization group analysis and numerical simulation of propagation and localization of acoustic waves in heterogeneous media

Alireza Bahraminasab,[1,*] S. Mehdi Vaez Allaei,[1,2] Farhad Shahbazi,[3] Muhammad Sahimi,[4,†] M. D. Niry,[5] and M. Reza Rahimi Tabar[5,6,‡]

[1]*International Center for Theoretical Physics, Strada Costiera 11, I-34100 Trieste, Italy*

[2]*Institute for Advanced Studies in Basic Sciences, Gava Zang, Zanjan 45195-1159, Iran*

[3]*Department of Physics, Isfahan University of Technology, Isfahan 84156, Iran*

[4]*Mork Family Department of Chemical Engineering and Materials Science, University of Southern California, Los Angeles, California 90089-1211, USA*

[5]*Department of Physics, Sharif University of Technology, Tehran 11365, Iran*

[6]*CNRS UMR 6529, Observatoire de la Côte d'Azur, BP 4229, 06304 Nice Cedex 4, France*

(Received 2 March 2006; revised manuscript received 19 November 2006; published 1 February 2007)

Propagation of acoustic waves in strongly heterogeneous elastic media is studied using renormalization group analysis and extensive numerical simulations. The heterogeneities are characterized by a broad distribution of the local elastic constants. We consider both Gaussian-white distributed elastic constants, as well as those with long-range correlations with a nondecaying power-law correlation function. The study is motivated in part by recent analysis of experimental data for the spatial distribution of the elastic moduli of rock at large length scales, which indicated that the distribution contains the same type of long-range correlations as what we consider in the present paper. The problem that we formulate and the results are, however, applicable to acoustic wave propagation in any disordered elastic material that contains the types of heterogeneities that we consider in the present paper. Using the Martin-Siggia-Rose method, we analyze the problem analytically and find that, depending on the type of disorder, the renormalization group (RG) flows exhibit a transition to a localized or extended regime in *any* dimension. We also carry out extensive numerical simulations of acoustic wave propagation in one-, two-, and three-dimensional systems. Both isotropic and anisotropic media (with anisotropy being due to stratified) are considered. The results for the isotropic media are consistent with the RG predictions. While the RG analysis, in its present form, does not make any prediction for the anisotropic media, the results of our numerical simulations indicate the possibility of the existence of a regime of *superlocalization* in which the waves' amplitudes decay as $\exp[-(|\mathbf{x}|/\xi)^{\gamma}]$, with $\gamma > 1$, where ξ is the localization length. However, further investigations may be necessary in order to establish the possible existence of such a localization regime.

DOI: 10.1103/PhysRevB.75.064301 PACS number(s): 62.65.+k, 71.23.An, 91.60.Lj, 47.56.+r

I. INTRODUCTION

Wave propagation in heterogeneous media is a fundamental phenomenon of great scientific and practical interest, and has been studied for a long time. It is relevant to such important problems as analyzing data for earthquakes and making predictions for their possible occurrence in the future, detecting underground nuclear explosions, understanding the large-scale structure of oil, gas, and geothermal reservoirs, gaining insight into what happens at large depths in the oceans, and designing instruments that are used for medical imaging, and characterizing materials.[1,2] For example, seismic wave propagation and reflection are used to not only estimate the hydrocarbon content of a potential oil reservoir, but also the spatial distributions of its fractures, faults, and strata, as well as its porosity.[3] More generally, they are used to image structures located over a wide area, ranging from the Earth's near surface to the deeper crust and upper mantle.

The purpose of the present paper is to study the effect of strong heterogeneities, represented by a spatial distribution of the local elastic constants, on wave propagation in disordered media. An important example of such media is rock, which represents a highly heterogeneous natural material. Recently, extensive experimental data for the spatial distributions of the local elastic moduli, the densities, and the wave velocities in several large-scale porous rock formations, both off- and onshore, were analyzed.[4] The analysis indicated[4] the existence of long-range correlations in the spatial distributions of the measured quantities, characterized by *nondecaying* power-law correlation functions. The existence of such correlations in the data provided the impetus for the present study and motivated an important question that we address in the present paper: How do such large-scale and strong heterogeneities and long-range correlations affect wave propagation in elastic media, and in particular in rock?

To better understand the problem that we wish to study in this paper, consider seismic wave propagation in rock.[4] In a seismic experiment (typically carried out by creating an explosion on the ground) for, for example, exploration, rock's heterogeneities (represented by the spatial distributions of its elastic constants, the porosity, the anisotropy caused by stratification, and existence of fractures and faults) cause multiple scattering and interference of the waves. The second question that we would like to address in the present paper is, whether the heterogeneities and the associated scattering and interference effects can give rise to *localization* of the waves. By localization we mean a situation in which, over

finite length scales (which could, however, be large), the waves' amplitude decays and essentially vanishes.

If the waves do localize (in the sense defined above), they would have important practical implications. For example, a main goal of a seismic exploration is to gain information on the morphology of rock (in addition to its contents), i.e., the spatial distributions of its porosity, faults, fractures, and strata. However, localization of seismic waves in the rock would imply that such information can be obtained only over distances r from the explosion's site that are of the order of the localization length ξ. In other words, if, for example, ξ is on the order of a few kilometers, but the linear size of an oil reservoir for which the seismic exploration is done is significantly larger than ξ, seismic recordings can, at best, provide only partial information on the reservoir, over length scales that are smaller than ξ.

As another example, consider the analysis of the seismic waves that are emanated by an earthquake in rock. If the station that collects data for such waves is at a distance from the earthquake's hypocenter which is larger than the localization length of the propoagating seismic wave in the rock, no useful information on the seismic activity prior to and during the earthquake can be gleaned from the data, as they should represent only noise, and not carry much useful information.

To put the problem that we study in this paper in a familiar context, we recall a well-known phenomenon in condensed matter physics, namely, the nature of electronic states in heterogeneous materials.[5] It is now well-known and well-understood that the answer to the question of whether electrons in a given material are localized or are in an extended state depends strongly on the material's spatial dimensionality d and the state of its heterogeneity. In one-dimensional (1D) materials, even weak disorder, irrespective of the energy, localizes the wave function.[6] The wave function $\psi(r)$ decays exponentially at large distances r from the domain's center, $\psi(r) \sim \exp(-r/\xi)$, where ξ is the localization length. In fact, the scaling theory of localization[7] predicts that, for $d \leqslant 2$, all electronic states are localized for any degree of disorder, but a transition to extended states occurs for $d > 2$, depending on the strength of the disorder. The transition between the two states—the metal-to-insulator transition—is characterized by divergence of ξ according to, $\xi \propto |W - W_c|^{-\nu}$, where W_c is the critical value of the disorder intensity. Both the scaling theory and the field-theoretic formulation of the electron localization problem by Wegner[8] predict that the lower critical dimension for the localization problem is, $d_c = 2$. Over the years, extensive numerical simulations have also been carried out to confirm such predictions; see, for example, Kramer and MacKinnon[9] for a review.

An important implication of the wave characteristics of electrons is that, the localization phenomenon may also occur in propagation of classical waves in disordered media. This observation provided another motivation for our study. However, unlike the problem of electron localization in strongly heterogeneous materials which has proven to be very difficult to study,[10] classical waves,[11] such as seismic waves, do not interact with one another and, therefore, their propagation in such highly heterogeneous media as natural rock provides an ideal model for studying the localization phenomenon.

Thus, as the first step toward the eventual goal of studying propagation of elastic waves in strongly heterogeneous solids, we study in this paper propagation of acoustic waves in the same type of media in which the heterogeneities, represented by the spatial distribution of the local elastic constants, are broadly distributed. We consider both a random distribution of the local elastic constants and also, consistent with the recent results,[4] a correlated distribution with a power-law, nondecaying correlation function, and investigate the possibility of localization of acoustic waves in such disordered solids.

The problem is studied by two different methods. First, we formulate a field-theoretic method to investigate acoustic wave propagation in disordered media that are characterized by a broad distribution of the elastic constants. Our approach is based on the method first introduced by Martin, Siggia, and Rose (MSR) (Ref. 12) for analyzing dynamical critical phenomena. We calculate the one-loop β functions[12] for both spatially random and power-law correlated distribution of the local elastic constants. Next, we present the results of extensive numerical simulation of acoustic wave propagation in the same disordered media in one (1D), two (2D), and three dimensions (3D), and show that in any case there is a disorder-induced transition from delocalized to localized states for *any* spatial dimension d. The preliminary results of our work were presented in a recent paper.[13] In the present paper, we provide full details of our renormalization group (RG) analysis, which is quite complex, and present extensive numerical results. Although our work was primarily motivated by the analysis of experimental data for the spatial distribution of elastic constants of rock at large scales,[4] the results presented in this paper are general and apply to any solid material in which the local elastic constants are distributed broadly, and follow the statistics of the distributions that we consider.

We point out that theoretical studies of localization of acoustic waves were previously carried out by several groups.[14–17] For example, Baluni and Willemsen[16] studied propagation of acoustic waves in a 1D layered system, composed of blocks of different elastic constants in series, and showed that the waves are localized. In addition, there have been several experimental studies of these problems in various disordered media.[18,19] However, the previous theoretical studies did not consider the problem in the type of strongly disordered media that we consider in this paper, which represent the continuum limit of an acoustic system with *off-diagonal* disorder, and also not in the context of the issues that are of interest to us. In addition, the dynamical RG method that we utilize[13] had not been used before.

The rest of this paper is organized as follows. In Sec. II we present a MSR formulation for the propagation of acoustic waves in heterogeneous media, and perform a perturbative RG calculation based on the MSR action. In Sec. III we discuss the physical implications of the RG results, while the analytical calculations by the RG method are tested in Sec. IV by carrying out extensive numerical simulations. The results are summarized in Sec. V.

II. RENORMALIZATION GROUP ANALYSIS

Acoustic waves propagate in elastic solids, and viscous and inviscid fluids,[1,20] although only the former type of media is of interest to us in this paper. To study acoustic wave propagation in an elastic medium with a distribution of elastic constants, we analyze the scalar wave equation (Refs. 1 and 20):

$$\frac{\partial^2}{\partial t^2}\psi(\mathbf{x},t) - \boldsymbol{\nabla}\cdot[\lambda(\mathbf{x})\,\boldsymbol{\nabla}\,\psi(\mathbf{x},t)] = 0, \tag{1}$$

where $\psi(\mathbf{x},t)$ is the wave amplitude (a complex quantity), t is the time, and $\lambda(\mathbf{x})=e(\mathbf{x})/m$ the ratio of the elastic stiffness $e(\mathbf{x})$ and the medium's mean density m. Equation (1) is valid in any dimension d ($d=1,2$, and 3). Usually, propagation of the P waves in an elastic medium is described by Eq. (1).[1,20] Real disordered solids support the propagation of both P and S waves. But, as mentioned in the Introduction, the present study represents a first concrete step toward the eventual goal of studying propagation of elastic waves in the type of disordered solid media that we consider in the present paper.

To introduce the spatial distribution of $\lambda(\mathbf{x})$ and its correlation function into the analysis, we write λ as follows,

$$\lambda(\mathbf{x}) = \lambda_0 + \eta(\mathbf{x}), \tag{2}$$

where $\lambda_0=\langle\lambda(\mathbf{x})\rangle$. In the present paper $\eta(\mathbf{x})$ is assumed to be a Gaussian random process with a zero mean and the covariance,

$$\langle\eta(\mathbf{x})\,\eta(\mathbf{x}')\rangle = 2C(|\mathbf{x}-\mathbf{x}'|) = 2D_0\delta^d(\mathbf{x}-\mathbf{x}') + 2D_\rho|\mathbf{x}-\mathbf{x}'|^{2\rho-d}, \tag{3}$$

in which D_0 and D_ρ represent, respectively, the strength of the disorder due to the delta-correlated and power-law correlated parts of the disorder. Previously, Souillard and co-workers[15] studied wave propagation in disordered *fractal* media, the *geometry* (connectivity) of which was characterized by a *decaying* power-law correlation function, whereas in the present problem we make no reference to the system's geometry, and consider power-law correlation functions only for the local elastic constants. Thus, their study is not related to our work.

Before proceeding further, let us point out that the spatial-dependence of electron localization, while sharing some similarity with localization of classical waves, may not necessarily be identical with localization of acoustic waves. The equation that we use—the scalar wave equation given above—is obviously not identical with the Schrödinger equation. Moreover, there are some basic differences between the two equations. For example, whereas Eq. (1) is invariant under time reversal, i.e., under the transformation $t\rightarrow -t$, there is no such symmetry in the Schrödinger equation. In addition, the Schrödinger equation contains an extra parameter—the mass—which must be carefully taken into account in any RG analysis. In the analysis that follows, the average $\langle\lambda_0\rangle$ plays the role of mass, but with the difference that, as we show below, the RG analysis can handle it in a straightforward manner.

Consider a wave component with angular frequency ω by taking the temporal Fourier transformation of $\psi(\mathbf{x},t)$,

$$\psi(\mathbf{x},\omega) = \frac{1}{(2\pi)^d}\int dt\,\exp(i\omega t)\psi(\mathbf{x},t). \tag{4}$$

Equation (1) then yields the following equation for the propagation of a wave component with a frequency ω:

$$f(\psi) = \nabla^2\psi(\mathbf{x},\omega) + \frac{w^2}{\lambda_0}\psi(\mathbf{x},\omega) + \boldsymbol{\nabla}\cdot\left[\frac{\eta(\mathbf{x})}{\lambda_0}\,\boldsymbol{\nabla}\,\psi(\mathbf{x},\omega)\right] = 0. \tag{5}$$

The Gaussian nature of the noise $\eta(\mathbf{x})$ leads us to write the following *generating functional* for wave function:

$$P[\psi_R,\psi_I,\eta] \sim \int D\eta D\psi_R D\psi_I \delta[f(\psi_R)]\delta[f(\psi_I)] \times J\left[\frac{\partial f(\psi_R)}{\partial\psi_R}\right] J\left[\frac{\partial f(\psi_I)}{\partial\psi_I}\right] \times\exp\left[-\int d\mathbf{x}d\mathbf{x}'\,\eta(\mathbf{x})D(\mathbf{x}-\mathbf{x}')\,\eta(\mathbf{x}')\right], \tag{6}$$

where $\psi_R(\mathbf{x})$ and $\psi_I(\mathbf{x})$ are, respectively, the real and imaginary components of the wave function [both satisfying Eq. (1)], and $D(\mathbf{x}-\mathbf{x}')$ is the inverse function of correlation function $C(\mathbf{x}-\mathbf{x}')$ that satisfies the following equation:

$$\int d\mathbf{x}'\,C(\mathbf{x}-\mathbf{x}')D(\mathbf{x}'-\mathbf{x}'') = \delta(\mathbf{x}-\mathbf{x}'). \tag{7}$$

In Eq. (6), $J[\partial f(\psi_R)/\partial\psi_R]$ and $J[\partial f(\psi_I)/\partial\psi_I]$ are the Jacobians given by

$$J = \det\left\{\frac{\partial f[\psi(\mathbf{x})]}{\partial\psi(\mathbf{x}')}\right\} = \det\left\{\nabla^2\delta(\mathbf{x}-\mathbf{x}') + \frac{w^2}{\lambda_0}\delta(\mathbf{x}-\mathbf{x}') + \boldsymbol{\nabla}\cdot\left[\frac{\eta(\mathbf{x})}{\lambda_0}\,\boldsymbol{\nabla}\,\delta(\mathbf{x}-\mathbf{x}')\right]\right\}. \tag{8}$$

Using the MSR method,[12] we write the delta function as a Gaussian integral over an auxiliary field $\tilde{\psi}_R(\mathbf{x})$ and $\tilde{\psi}_I(\mathbf{x})$. On the other hand, using the integral representation of the determinant by the anticommuting variables, we can also write the Jacobian as a Gaussian integral over the Grassmanian fields χ and χ^* (where * indicates a complex-conjugate property). Therefore, Eq. (6) is rewritten

$$P[\psi,\psi,\chi,\chi^*,\eta] \sim \int [D\psi][D\tilde{\psi}][D\chi][D\chi^*][D\eta]\exp[- S(\psi,\tilde{\psi},\chi,\chi^*,\eta)], \tag{9}$$

where the action $S(\psi,\tilde{\psi},\chi,\chi^*,\eta)$ is given by,

$$S = \int d\mathbf{x}d\mathbf{x}' \Bigg[i\tilde{\psi}_R(\mathbf{x}')\left(\nabla^2 + \frac{w^2}{\lambda_0}\right)\psi_R(\mathbf{x}) + i\tilde{\psi}_I(\mathbf{x}')\left(\nabla^2 + \frac{w^2}{\lambda_0}\right)\psi_I(\mathbf{x}) - i\frac{\eta}{\lambda_0}(\mathbf{x})\,\nabla\,\tilde{\psi}_R(\mathbf{x}')\,\nabla\,\psi_R(\mathbf{x}) - i\frac{\eta}{\lambda_0}(\mathbf{x})\,\nabla\,\tilde{\psi}_I(\mathbf{x}')\,\nabla\,\psi_I(\mathbf{x})$$
$$+ \chi_R^*(\mathbf{x}')\left(\nabla^2 + \frac{w^2}{\lambda_0}\right)\chi_R(\mathbf{x}) + \chi_I^*(\mathbf{x}')\left(\nabla^2 + \frac{w^2}{\lambda_0}\right)\chi_I(\mathbf{x}) - \frac{\eta}{\lambda_0}(\mathbf{x})\,\nabla\,\chi_R^*(\mathbf{x}')\,\nabla\,\chi_R(\mathbf{x}) - \frac{\eta}{\lambda_0}(\mathbf{x})\,\nabla\,\chi_I^*(\mathbf{x}')\,\nabla\,\chi_I(\mathbf{x})\Bigg]\delta(\mathbf{x}-\mathbf{x}')$$
$$- \eta(\mathbf{x})D(\mathbf{x}-\mathbf{x}')\eta(\mathbf{x}'). \tag{10}$$

Using simple Gaussian integration we integrate η out in Eq. (9) to obtain

$$P[\psi,\tilde{\psi},\chi,\chi^*] \sim \int [D\psi][D\tilde{\psi}][D\chi][D\chi^*]\exp\{-S_e[\psi,\tilde{\psi},\chi,\chi^*]\}, \tag{11}$$

in which the effective action S_e is given by,

$$S_e(\psi,\tilde{\psi},\chi,\chi^*) = \int d\mathbf{x}d\mathbf{x}' \Bigg[\left(i\tilde{\psi}_I(\mathbf{x}')\left(\nabla^2 + \frac{\omega^2}{\lambda_0}\right)\psi_I(\mathbf{x}) + i\tilde{\psi}_R(\mathbf{x}')\left(\nabla^2 + \frac{\omega^2}{\lambda_0}\right)\psi_R(\mathbf{x})\right)\delta(\mathbf{x}-\mathbf{x}')\Bigg]$$
$$+ \left(\chi_I^*(\mathbf{x}')\left(\nabla^2 + \frac{\omega^2}{\lambda_0}\right)\chi_I(\mathbf{x}) + \chi_R^*(\mathbf{x}')\left(\nabla^2 + \frac{\omega^2}{\lambda_0}\right)\chi_R(\mathbf{x})\right)\delta(\mathbf{x}-\mathbf{x}') + (i\,\nabla\,\tilde{\psi}_I\,\nabla\,\psi_I + i\,\nabla\,\tilde{\psi}_R\,\nabla\,\psi_R$$
$$+ \nabla\chi_I^*\,\nabla\,\chi_I + \nabla\chi_R^*\,\nabla\,\chi_R)\frac{C(\mathbf{x}-\mathbf{x}')}{\lambda_0^2}\ (i\,\nabla\,\tilde{\psi}_I\,\nabla\,\psi_I + i\,\nabla\,\tilde{\psi}_R\,\nabla\,\psi_R + \nabla\chi_I^*\,\nabla\,\chi_I + \nabla\chi_R^*\,\nabla\,\chi_R)]. \tag{12}$$

Two coupling constants, $g_0 = D_0/\lambda_0^2$, and, $g_\rho = D_\rho/\lambda_0^2$, appear in S_e, when we substitute Eq. (3) for the function $C(\mathbf{x}-\mathbf{x}')$ into Eq. (12) (see Fig. 1). Thus, carrying out a RG analysis in the critical limit, $\omega^2/\lambda_0 \to 0$, we derive, to one-loop order, the beta functions[12] that govern the two coupling constants under the RG transformation.

There is an intuitively appealing diagrammatic representation of the terms that appear in the perturbative evaluation of the rescaling in the RG analysis, which is shown in Fig. 2. We show in Fig. 3 all the diagrams that contribute to the four-point correlation function term, $\langle\psi_R(\mathbf{x}_1)\tilde{\psi}_R(\mathbf{x}_2)\psi_R(\mathbf{x}_3)\tilde{\psi}_R(\mathbf{x}_4)\rangle$, to one-loop order. There are also ten vertices that contribute to renormalization of g_0 and g_ρ. Figure 4 indicates that the following expression holds for I_2 in the hydrodynamic limit, $\omega/\lambda_0 \to 0$,

$$I_2 = \frac{16g_0^2}{\left(\frac{k^2}{2} - k_1^2\right)\left(\frac{k^2}{2} - k_2^2\right)}\int d\mathbf{q}\frac{\left[\mathbf{q}\cdot\left(\frac{\mathbf{k}}{2} + \mathbf{k}_1\right)\right]\left[\mathbf{q}\cdot\left(\frac{\mathbf{k}}{2} - \mathbf{k}_1\right)\right]\left[(\mathbf{q}+\mathbf{k}_1+\mathbf{k}_2)\cdot\left(\frac{\mathbf{k}}{2} + \mathbf{k}_2\right)\right]\left[(\mathbf{q}+\mathbf{k}_1+\mathbf{k}_2)\cdot\left(\frac{\mathbf{k}}{2} - \mathbf{k}_2\right)\right]}{\left(q^2 - i\frac{\omega}{\lambda_0}\right)\left[(\mathbf{q}+\mathbf{k}_1+\mathbf{k}_2)^2 + i\frac{\omega}{\lambda_0}\right]}. \tag{13}$$

$\mathbf{q}$ is calculated in spherical coordinates. We use, $\mathbf{k}_i\cdot\mathbf{q} = kq\cos\theta_i$, where θ_i is the angle between $\mathbf{q}$ and $\mathbf{k}_i$, which yield,

$$I_2 = \frac{16g_0^2}{\left(\frac{k^2}{2} - k_1^2\right)\left(\frac{k^2}{2} - k_2^2\right)}\frac{S_{d-1}}{2\pi^d}\int dq q^{d-1}\int d\theta_1 \sin^{d-2}\theta$$
$$\times\frac{\left[\left(\frac{kq\cos\theta}{2} + k_1 q\cos\theta_1\right)\right]\left[\left(\frac{kq\cos\theta}{2} - k_1 q\cos\theta_1\right)\right]\left[\left(\frac{kq\cos\theta}{2} + k_2 q\cos\theta_2\right)\right]\left[\left(\frac{kq\cos\theta}{2} + k_2 q\cos\theta_2\right)\right]}{\left(q^2 - i\frac{\omega}{\lambda_0}\right)\left[(\mathbf{q}+\mathbf{k}_1+\mathbf{k}_2)^2 + i\frac{\omega}{\lambda_0}\right]}$$
$$= 16g_0^2 k_d\left[\frac{d+5}{2d(d+2)}\right]\int dq q^{d-1}, \tag{14}$$

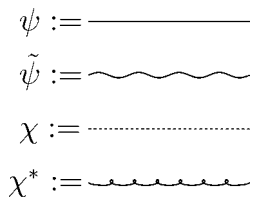

FIG. 1. Diagrammatic representations of the fields appearing in the effective action, Eq. (12).

with $k_d = S_d/(2\pi^d)$, and S_d being the surface area of the d-dimensional unit sphere. Thus, we find that

$$I_1 = 16 g_0^2 k_d \left[\frac{d+5}{2d(d+2)}\right] \int dq q^{d-1},$$

$$I_3 = -4 g_0^2 k_d \left[\frac{d+5}{2d(d+2)}\right] \int dq q^{d-1},$$

$$I_4 = 16 g_0 g_\rho k_d \left[\frac{d+5}{2d(d+2)}\right] \int dq q^{d-1} q^{-2\rho},$$

$$I_5 = 16 g_0 g_\rho k_d \left[\frac{d+5}{2d(d+2)}\right] \int dq q^{d-1} q^{-2\rho},$$

$$I_6 = 16 g_\rho^2 k_d \left[\frac{d+5}{2d(d+2)}\right] \int dq q^{d-1} q^{-4\rho},$$

$$I_7 = 16 g_\rho^2 k_d \left[\frac{d+5}{2d(d+2)}\right] \int dq q^{d-1} q^{-4\rho},$$

$$I_8 = 16 g_0 g_\rho k_d \left[\frac{d+5}{2d(d+2)}\right] k^{-2\rho} \int dq q^{d-1},$$

$$I_9 = -4 g_0 g_\rho k_d \left[\frac{d+5}{2d(d+2)}\right] k^{-2\rho} \int dq q^{d-1},$$

FIG. 2. Diagrammatic representations of the propagators and vertices in the effective action S_e. $\mathbf{k}$ is the momentum transfer from left to right.

$$I_{10} = 16 g_0 g_\rho k_d \left[\frac{d+5}{2d(d+2)}\right] k^{-2\rho} \int dq q^{d-1} q^{-2\rho}. \quad (15)$$

It is also straightforward to determine that the dimensions of parameters under a change of scale, $x \to bx$, are:

$$[g_0] = d, \quad (16)$$

$$[g_\rho] = d - 2\rho. \quad (17)$$

The functions $\beta(\tilde{g}_0)$ and $\beta(\tilde{g}_\rho)$ are then given by,

$$\beta(\tilde{g}_0) = \frac{\partial \tilde{g}_0}{\partial \ln l} = -d\tilde{g}_0 + 8\tilde{g}_0^2 + 10\tilde{g}_\rho^2 + 20\tilde{g}_0\tilde{g}_\rho, \quad (18)$$

$$\beta(\tilde{g}_\rho) = \frac{\partial \tilde{g}_\rho}{\partial \ln l} = (2\rho - d)\tilde{g}_\rho + 12\tilde{g}_0\tilde{g}_\rho + 16\tilde{g}_\rho^2, \quad (19)$$

where $l > 1$ is the rescaling parameter, and

$$\tilde{g}_0 = k_d \left[\frac{d+5}{2d(d+2)}\right] g_0, \quad (20)$$

$$\tilde{g}_\rho = k_d \left[\frac{d+5}{2d(d+2)}\right] g_\rho, \quad (21)$$

with $k_d = S_d/(2\pi^d)$.

III. IMPLICATIONS OF THE RG RESULTS

The beta functions that we have determined, Eqs. (18) and (19), describe how the two couplings—g_0 and g_ρ—behave, if

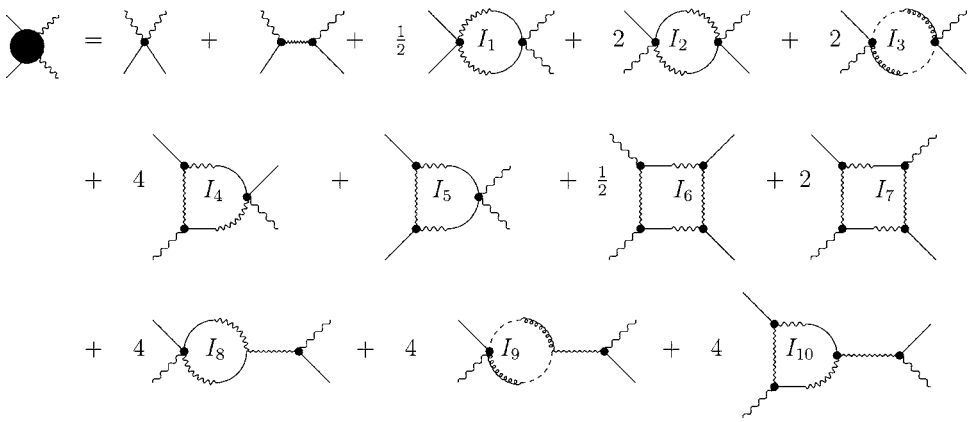

FIG. 3. One-loop corrections to the four-point correlation function.

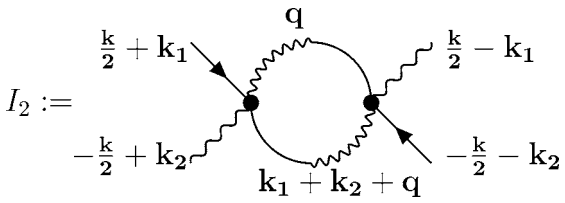

FIG. 4. Feynman diagram of integral I_2.

we rescale all the lengths and consider the elastic medium at coarser scales. If we find, for example, that a small g_0 diverges under the RG rescaling, it implies that a small g_0 at small length scales behaves as very strong disorder at much larger scales and, therefore, every wave amplitude will be localized. If, on the other hand, we find, for example, that for some $g_0 < g_c$ (where g_c is a critical value of g_0) g_0 vanishes under the RG rescaling, it implies that in this regime g_0 does not contribute much to the behavior of the propagating waves at large length scales. Therefore, a localized state may be defined as follows: we have localized states if, under the RG rescaling, *at least* either g_0 or g_ρ diverges.

To understand better the predictions of the RG analysis, we examine the RG flows, Eqs. (6) and (7), which reveal that, depending on ρ, there can be two distinct regimes:

(i) For $0 < \rho < \frac{1}{2}d$ there are three sets of fixed points: The trivial set representing the Gaussian fixed points, $g_0^* = g_\rho^* = 0$, which is stable, and two other sets representing nontrivial fixed points and the corresponding eigendirections. One is, $\{g_0^* = \frac{1}{8}d, g_\rho^* = 0\}$, while the other set is given by,

$$g_0^* = -\frac{4}{41}\left[d + \frac{5}{16}(2\rho - d)\right] - \frac{4}{41}\sqrt{\left[d + \frac{5}{16}(2\rho - d)\right]^2 + \frac{205}{256}(2\rho - d)^2},$$

$$g_\rho^* = \frac{3}{4}g_0^* + \frac{1}{16}(d - 2\rho), \tag{22}$$

which is stable in one eigendirection but unstable in the other eigendirection. The corresponding RG flow diagram is shown in Fig. 5. Therefore, for $0 < \rho < \frac{1}{2}d$ the one-loop RG

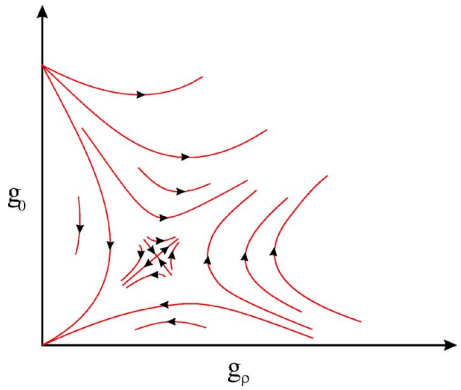

FIG. 5. (Color online) Flows in the coupling constants space for $0 < \rho < \frac{1}{2}d$.

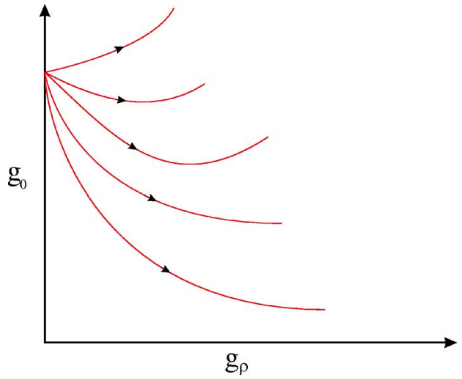

FIG. 6. (Color online) Flows in the coupling constants space for $\rho > \frac{1}{2}d$.

analysis indicates that a medium with uncorrelated disorder is unstable against long-range correlated disorder towards a new fixed point in the space of the coupling constants. Hence, there is a phase transition from delocalized to localized states with increasing the disorder intensity.

Thus, the physical implication of the RG results becomes clear. Figure 5 indicates that, in the interval $0 < \rho < \frac{1}{2}d$, there is a region in the space of the coupling constants $\{g_0, g_\rho\}$ in which the RG flows take any initial point to the Gaussian fixed point, $\{g_0 = g_\rho = 0\}$. This indicates that, in this region, a disordered medium of the type considered in this paper looks like a pure (nondisordered or homogeneous) medium at large length scales, implying that the wave is *extended* or delocalized.

However, when g_0 or g_ρ are large enough that the initial point is out of the basin of attraction of the Gaussian fixed point, the RG flow moves such points toward large values, hence implying that, under the RG rescaling, the probability density function of the disorder becomes broader and broader at larger and larger length scales. Therefore, in this case, a propagating wave samples a medium with a very large spatial fluctuation in the elastic stiffness or moduli. Moreover, note that even if one starts in a disordered medium with purely long-range correlations (i.e., one with $g_0 = 0$), one finds from the RG equations that the growth of g_ρ will lead to increasing, i.e., *nonzero*, g_0, hence implying that *uncorrelated* disorder will be produced by the RG rescaling. Since the local fluctuations in the bulk moduli (and, more generally, the local stiffness) play the role of scattering points, the implication is that the multiple scattering of a propagating wave from the uncorrelated disorder will destroy the wave's coherence, leading eventually to its localization. This is the basis of the localization-delocalization transition in the low frequency limit, in terms of the disorder intensity.

(ii) For $\rho > \frac{1}{2}d$ there are two fixed points: the Gaussian fixed point which is stable on the g_0 axis but not on the g_ρ axis, and the nontrivial fixed point, $\{g_0^* = \frac{1}{8}d, g_\rho^* = 0\}$, which is unstable in all directions. The corresponding RG flow diagram is shown in Fig. 6. The implication is that, although power-law correlated disorder is relevant, no new fixed point exists to one-loop order and, therefore, the system's long-wavelength behavior is determined by the long-range component of the disorder. This implies that for $\rho > \frac{1}{2}d$ the waves

are localized for *any d*. In addition, in both cases the system undergoes a disorder-induced transition when only the uncorrelated disorder is present.

Let us mention that the above results are general so long as $D_\rho > 0$ (which is the only physically acceptable limit). For $D_\rho < 0$ the above phase space is valid for $\rho > \frac{1}{2}(d+1)$.

We also point out that, it is convenient to begin the RG rescaling and analysis with the assumption that the couplings g_0 and g_ρ are small. If, under the RG rescaling, we find stable fixed points, it would imply that the assumption of the couplings being small about such a fixed point is still valid. However, around the unstable fixed point the couplings can grow and, hence, the perturbation that we have developed would fail. But, for our purpose, i.e., to determine the localized/extended regimes, the most important goal is to determine the condition(s) under which the fixed points are unstable, so that the couplings can diverge.

Although the above RG calculations were carried out to one-loop order, the analysis will still be valid for higher orders of the perturbation as well, since it should be clear that the signs of the higher-order terms are all positive. That this is so due to the following. We must keep in mind that the contraction coefficients for auxiliary fields are always greater than those of auxiliary *and* Grassmanian fields, that supply the negative terms. Moreover, the numbers of diagrams of, e.g., a real auxiliary field and an imaginary auxiliary field are equal to the number of diagrams of an auxiliary *and* Grassmanian field. This implies immediately that the signs of higher-order terms should also be positive.

IV. NUMERICAL SIMULATIONS

To test the predictions of the RG analysis, we have carried out numerical simulations of the problem in 1D, 2D, and 3D systems. In what follows we describe the techniques that we used for the numerical simulation of the problem in 1D systems on the one hand, and 2D and 3D systems on the other hand, which are quite distinct. We then describe and discuss the numerical results.

A. One-dimensional media

An experimental realization of a simple 1D model that exhibited wave localization was presented by He and Maynard.[18] It consisted of a 15 m long steel wire, suspended vertically, with a diameter of 0.178 mm. The tension in the wire was maintained with a weight attached at its lower end. Then, the function $\psi(x,t)$ corresponds to transverse waves in the wire with an electromechanical actuator at one end of the wire. It was demonstrated[18] that, even for very small deviations (less than 1%) from periodicity, the diagonal disorder, represented by, e.g., variations in the resonance frequencies of the oscillators, produces localization, which agrees with Furstenberg's theorem.[21] On the other hand, variations (of up to 13%) in the masses, representing off-diagonal disorder, resulted in localization lengths that were much larger than the system's size. This is in agreement with the RG prediction presented here.

To reproduce numerically the results of He and Maynard[18] for 1D systems, to confirm the RG prediction, and to calculate the localization length ξ, we used the transfer-matrix (TM) method of Soukoulis, Economou, Grest, and Cohen.[9] Discretizing the 1D version of Eq. (1), and writing down the result for site n of a linear chain yields,

$$\left[\lambda\frac{\partial\psi}{\partial x}\right]_{n+(1/2)} - \left[\lambda\frac{\partial\psi}{\partial x}\right]_{n-(1/2)} + \omega^2\psi_n = 0, \tag{23}$$

and

$$\lambda_{n+(1/2)}(\psi_{n+1} - \psi_n) - \lambda_{n-(1/2)}(\psi_n - \psi_{n-1}) + \omega^2\psi_n = 0. \tag{24}$$

Setting, $\lambda_{n+(1/2)} = \beta_{n+1}$, and $\lambda_{n-(1/2)} = \beta_n$, we rewrite Eq. (24) in the following recursive form;

$$\mathbf{M}_n\begin{pmatrix}\psi_n\\ \psi_{n-1}\end{pmatrix} = \begin{pmatrix}\psi_{n+1}\\ \psi_n\end{pmatrix} \tag{25}$$

with

$$\mathbf{M}_n = \begin{pmatrix}\dfrac{-\omega^2 + \beta_{n-1} + \beta_n}{\beta_n} & -\dfrac{\beta_{n-1}}{\beta_n}\\ 1 & 0\end{pmatrix}. \tag{26}$$

The localization length $\xi(\omega)$ is defined by, $\xi(\omega)^{-1} = \lim_{N\to\infty} N^{-1}\ln|\psi_N/\psi_0|$, where N is the chain's length (ξ^{-1} is sometimes referred to as the Lyapunov exponent). To check the existence of a nontrivial localization transition, we must consider a nonzero ω, even in the thermodynamic limit. The reason is that the mode $\omega = 0$ is related to the translational invariance of the system and has no physical importance.

The computations were carried out for many values of the system size N and frequency ω. For a system of a finite size N one has a minimum frequency, $\omega_m = 2\pi(\lambda_0)^{1/2}/N$, so that in the limit, $N\to\infty$, $\omega_m \to 0$, and one recovers the continuous limit. We used, $\lambda_0 = 10$ and took its random component, $\eta(x)$ [see Eq. (2)], to be a white noise with variance, $2D_0 = \sigma$. For every realization of the disorder we computed ψ_N and, hence, $\xi(\omega)$. We used, $\psi_0 = \psi_1 = 1/\sqrt{2}$, and carried out computations at selected values of ω. As shown in Refs. 22 and 23, in order to reduce the calculations' error, it is better to carry out the computations at frequencies, $\omega_{co} = N^{1/2}\omega_m = 2\pi\sqrt{\lambda_0}/N^{1/2}$, to check for the localization/delocalization transition. Every computed value of ξ represents an average over 6000 realizations for a fixed system size N and frequency ω.

Figure 7 presents the critical variance σ_c for the localization/delocalization transition, as a function of the system size N. It demonstrates clearly that, in the thermodynamic limit ($N\to\infty$), there is a nontrivial σ_c, such that for $\sigma < \sigma_c$ there is a phase transition. Fitting the numerical data for σ_c shown in Fig. 7 to an expression of the form,

$$\sigma_c = a + bN^{-\chi}, \tag{27}$$

where $a = \sigma_c(N\to\infty)$, we find that, $a \simeq 2.20 \pm 0.03$, $b \simeq 3.26 \pm 0.10$, and $\chi \simeq 0.18 \pm 0.01$.

We present in Fig. 8 the frequency dependence of $\xi(\omega)$ for $N = 6\times 10^6$ ($\sigma_c \simeq 2.34$) and three regimes, $\sigma > \sigma_c$, $\sigma = \sigma_c$, and

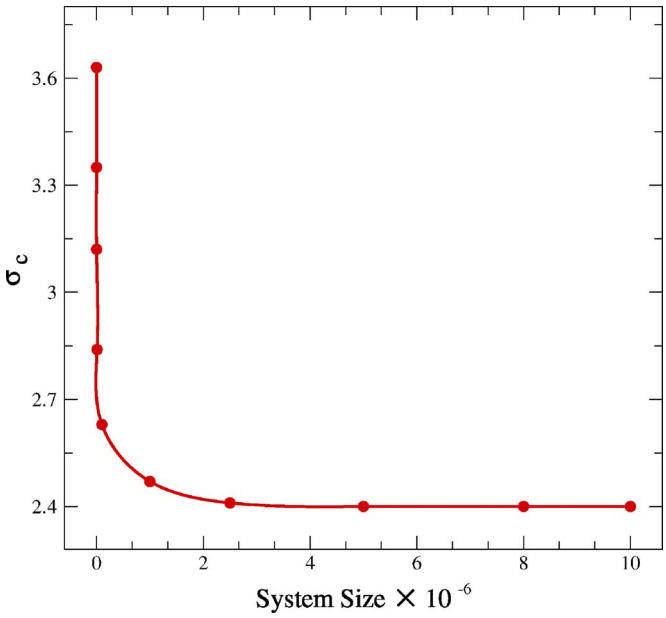

FIG. 7. (Color online) The critical variance σ_c as a function of system size N for white noise disorder. The results represent averages over 6000 realizations of the system.

$\sigma < \sigma_c$. In the limit, $\omega=0$ (and $N\to\infty$), the localization length ξ diverges, and the TM calculations shown in Fig. 8 confirm this expectation. For $\sigma < \sigma_c$, there are frequencies for which the localization length ξ is larger than the size N of the linear chain. Thus, in this regime of disorder and frequency modes the chain behaves like a metal in the classical localization. Increasing σ *reduces* the localization length ξ. Thus, for $\sigma = \sigma_c$ the lowest modes (which is ω_{co}, a cutoff frequency due to the finite-size effects) give rise to localization length of the order of the chain size N. Finally, for $\sigma > \sigma_c$ all the modes are localized. We also indicate in Fig. 8 where the localization lengths are comparable to the system size N for ω_{co}. These results are in agreement with the predictions of the RG analysis described above.

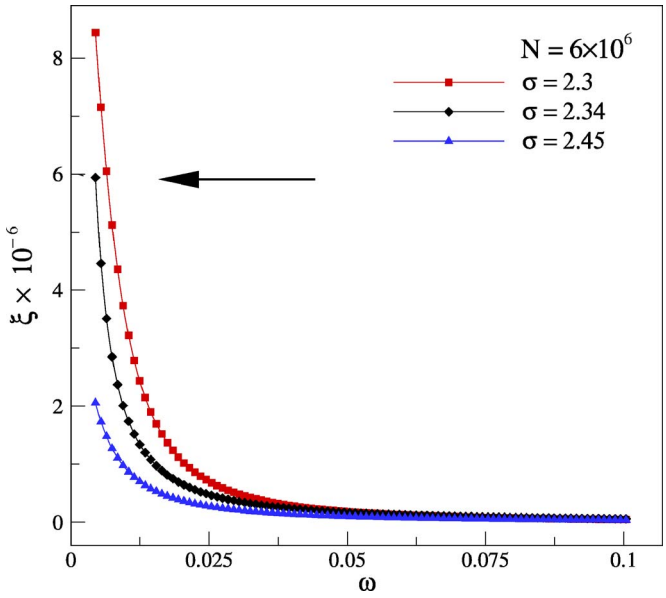

FIG. 8. (Color online) Localization length ξ as a function of the frequency ω for $\sigma < \sigma_c \simeq 2.4$ and $\sigma > \sigma_c$. The system size is $N=6\times10^6$. The results represent averages over 6000 realizations.

To further check the existence of the extended states for $\sigma < \sigma_c$ in the thermodynamic limit, one needs to check the condition $\lim_{N\to\infty}(\xi/N)=\text{constant}\neq 0$. If this condition is not satisfied, ξ becomes negligible in comparison with N in the thermodynamic limit ($N\to\infty$), and the wave amplitude would, therefore, be localized. Hence, we study the behavior of ξ as a function of N for two different values of the noise variance. As ξ is also a function of the wave frequency ω, we choose $\omega=\omega_{co}$, the cutoff frequency.

To carry out the computations, we solve the following eigenvalue problem,

$$\mathcal{H}|\Psi\rangle = -\omega^2|\Psi\rangle, \tag{28}$$

where,

$$\mathcal{H}_{m,n} = \lambda_{m+(1/2)}(\delta_{m+1,n} - \delta_{m,n}) - \lambda_{m-(1/2)}(\delta_{m,n} - \delta_{m-1,n}), \tag{29}$$

and diagonalize $\mathcal{H}$ to compute all the eigenvalues for different realization of the noise λ. We then approximate ω_{co} by the nearest ω (to within a small numerical window) in definition of the localization length ξ in terms of the transfer matrix M, i.e., $\xi(\omega)^{-1}=N^{-1}\langle \ln[\mathrm{Tr}(\Pi_{n=1}^{N} M_n)]\rangle$, and compute the localization length ξ. To avoid excessive numerical fluctuations, we average ξ in a small energy window around ω_{co}, and more specifically in the interval $[-0.01, 0.01]$. The averaging is taken over the realizations of the disorder. To compute the eigenvalues, we diagonalize the matrix representation of $\mathcal{H}$ and, using the QR factorization algorithm, compute all the eigenvalues of the real symmetric tridiagonal matrix.

We find a power-law relation between ξ and N, $\xi \propto N^{\gamma}$. This is shown in Fig. 9. The exponent γ seems to weakly depend on the disorder's variance, if at all. For $\sigma=0.1$ [i.e., less than $\sigma_c(N\to\infty)\simeq 2.20$], we find $\gamma=1$, while for $\sigma=5.0$ [greater than $\sigma_c(N\to\infty)\simeq 2.20$] we find, $\gamma=0.93\pm0.02$. These results confirm, once again, the predictions of the RG analysis for 1D disordered media.

B. Two- and three-dimensional media

We also carried out extensive numerical simulations in 2D and 3D systems by solving Eq. (1), using the finite-difference (FD) method with second-order discretization for the time and fourth-order discretization for the spatial variables. Consider, for example, the 2D systems. Using the FD approximation, we write $\psi(\mathbf{x},t)$ as $\psi_{i,j}^{(n)}$, where n denotes the time step number. The second-order FD approximation (accurate to Δt^2) to the time-dependent term of Eq. (1) is the standard form, $\partial^2\psi(\mathbf{x},t)/\partial t^2 \simeq (\psi_{i,j}^{(n+1)} - \psi_{i,j}^{(n)} + \psi_{i,j}^{(n-1)})/(\Delta t^2)$, where Δt is the time step's size. As for the spatial derivatives, we first expand the right side of Eq. (1) as follows:

$$\begin{aligned}\nabla\cdot[\lambda(\mathbf{x})\,\nabla\,\psi(\mathbf{x},t)] &= \nabla\lambda(\mathbf{x})\cdot\nabla\psi(\mathbf{x},t) + \lambda(\mathbf{x})\nabla^2\psi(\mathbf{x},t)\\ &= \partial_x\lambda(\mathbf{x})\partial_x\psi(\mathbf{x},t) + \partial_y\lambda(\mathbf{x})\partial_y\psi(\mathbf{x},t)\\ &\quad + \lambda(\mathbf{x})[\partial_x^2\psi(\mathbf{x},t) + \partial_y^2\psi(\mathbf{x},t)].\end{aligned}$$

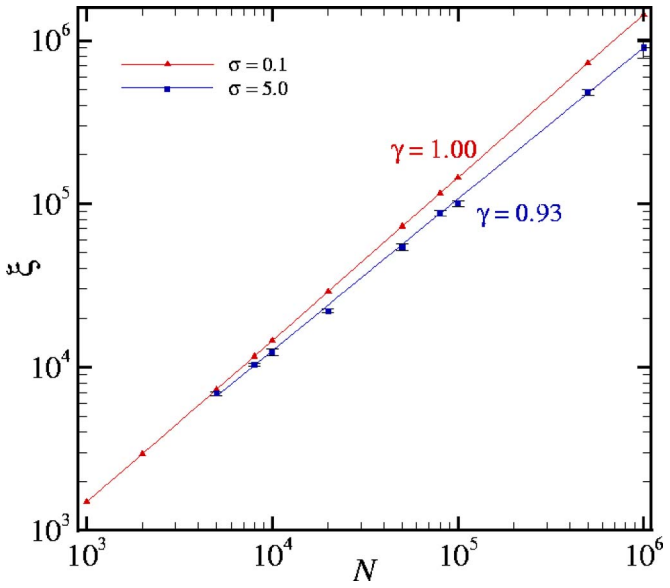

FIG. 9. (Color online) Test of the condition, $\lim_{N\to\infty}(\xi/N)$ = constant $\neq 0$ for the existence of the extended states for $\sigma<\sigma_c$ in the thermodynamic limit. We chose, $\omega=\omega_{co}$, and averaged ξ in a small energy window, $[-0.01, 0.01]$, around ω_{co}. The results indicate a power law, $\xi \propto N^{\gamma}$.

Then, using the fourth-order FD discretization, we obtain for, for example, the derivatives in the x direction,

$$\partial_x^2\psi(\mathbf{x},t) \simeq \frac{-\psi_{i+2,j}^{(n)} + 16\psi_{i+1,j}^{(n)} - 30\psi_{i,j}^{(n)} + 16\psi_{i-1,j}^{(n)} - \psi_{i-2,j}^{(n)}}{12\Delta x^2}, \tag{30}$$

and

$$\partial_x\psi(\mathbf{x},t) \simeq \frac{-\psi_{i+2,j}^{(n)} + 8\psi_{i+1,j}^{(n)} - 8\psi_{i-1,j}^{(n)} + \psi_{i-2,j}^{(n)}}{12\Delta x}, \tag{31}$$

where Δx is the spacing between two neighboring grid points in the x direction. Similar expressions are written down for the partial derivatives with respect to the y direction (and the z direction for the simulations in 3D). Such approximations proved to be accurate enough and provide the required stability to the numerical results, as we work in the limit of low frequencies or long wavelengths.[24] We used $L_x \times L_y$ grids in 2D with $L_x=8000$ and $L_y=400$ (where x is the main direction of wave propagation), and $L_x \times L_y \times L_z$ grids in 3D with $L_x = L_y = 70$, and $L_z=500$ (where z is the main direction of wave propagation). The parameter $\lambda(\mathbf{x})$, representing the gridblock-scale elastic constant, was distributed spatially with the power-law correlation function described above.

Two distinct classes of disordered media were considered. In one case, the disordered media studied were isotropic. In this case the spatial distribution of $\lambda(\mathbf{x})$ was generated using the midpoint displacement method[25] (we took $D_\rho=1.0$). In the second case, the media studied were anisotropic. While one may consider a variety of anisotropic systems, we considered, consistent with the structure of rock,[3] the anisotropy that is caused by stratification. Such disordered media contain layers with sharp contrasts between them. To generate the spatial distribution of the local elastic constants in the layered systems, we used a fast Fourier transformation technique.[26] A convenient representation of the distribution of $\lambda(\mathbf{x})$, the correlation function of which is of the power-law type given by Eq. (3), is through its power spectrum—the Fourier transform of its covariance—which is given by,

$$S(\boldsymbol{\omega}) = \frac{a(d)}{\left(\sum_i \omega_i^2\right)^{H+d/2}}, \tag{32}$$

where $a(d)$ is a d-dependent constant, and $\boldsymbol{\omega}=(\omega_1,\ldots,\omega_d)$, with ω_i being the Fourier component in the ith direction. Here, $H=\rho-1$ is the Hurst exponent with, $0\leqslant H\leqslant 1$, such that $H>1/2(<1/2)$ implies positive (negative) correlations among the increments of the values generated by the distribution, while $H=1/2$ is the usual Brownian (random) case. We rewrite the power spectrum in a more general form,

$$S(\boldsymbol{\omega}) = \frac{b(d)}{\left(\omega_c^2 + \sum_i a_i\omega_i^2\right)^{H+d/2}}, \tag{33}$$

where $b(d)$ is another d-dependent constant. The coefficients a_i are numerical constants such that with $a_i=1$ one recovers Eq. (32) for the isotropic case. For example, in 2D, setting $a_1\neq 1$ and $a_2=1$ generates strata that are parallel to direction 1. ω_c is a cutoff frequency such that for length scales $\ell<\ell_c=1/\omega_c$, the local elastic constants $\lambda(\mathbf{x})$ are correlated, whereas for $\ell>\ell_c$ they are random and uncorrelated. Thus, in addition to the isotropic systems, we also studied acoustic wave propagation in stratified media, as well as in those with a cutoff in the extent of the correlations. We also carried out simulations for the case in which values of $\lambda(\mathbf{x})$ were uncorrelated and uniformly distributed, but with the same variance as that of the power-law case.

To begin the simulations we start with a pulse wave source located at every node of the first row of the grid at $y=0$ (in 2D), or at every node of the xy plane at $z=0$ (in 3D). Such a boundary condition ensured generation of a smooth initial wave front. Using a point source will not change the results that we present below, although it would require a larger number of realizations for obtaining reliable statistics. As the source function $S(t)$ we used the following to generate the pulse waves (any other source may be used);

$$S(t) = -A(t-t_0)\exp[-\zeta(t-t_0)^2], \tag{34}$$

where A is a constant and ζ controls the wavelength of the wave. The discretized wave equation was then solved numerically throughout the system. Periodic boundary conditions were imposed in the lateral direction(s), which did not distort the nature of the wave propagation, as we used large system sizes. The discretized equations were integrated with up to 96 000 time steps in 2D and 24 000 time steps in 3D. The accuracy of the solution was checked by considering the stability criterion and the wavelength of the source.[24] To compute the amplitude decay in the medium, we collected the numerical results at 80 receivers (grid points), distributed evenly throughout the grid, along the main direction of wave propagation. The results were averaged over 45 realizations

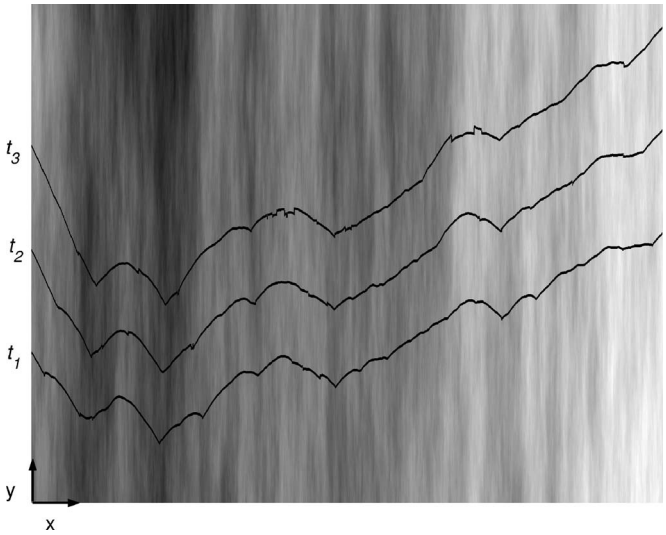

FIG. 10. The wave front in a 2D anisotropic system at (dimensionless) times, $t_1=328$, $t_2=384$, and $t_3=440$, with $\rho=1.5$.

of the system. The decay in the amplitude of the wave is caused by scattering of the wave by the system's heterogeneities generated by the spatial distribution of the local elastic constants.

Figure 10 shows the wave front (WF) at three different times in a 2D stratified medium with $\rho=1.5$. As the wave propagates, the roughness of the WF increases. The same qualitative patterns are observed in all the cases for $\rho>1.5$, except that the WFs become somewhat smoother, as the correlations in the local elastic constants for $\rho>1.5$ are positive and, therefore, there are extended zones of similar local elastic constants in the system.

Figure 11 presents the decay in the wave amplitude through a uniformly random 2D medium, and that of a 2D anisotropic medium with a nondecaying power-law correla-

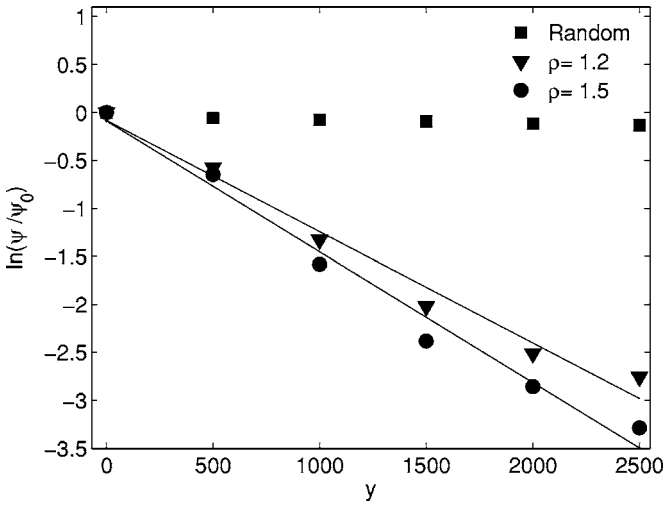

FIG. 11. Wave amplitudes in 2D anisotropic media, for both uniformly random and power-law correlated elastic constants. The main direction of wave propagation is parallel to the strata. The straight lines indicate that the amplitudes decay essentially exponentially.

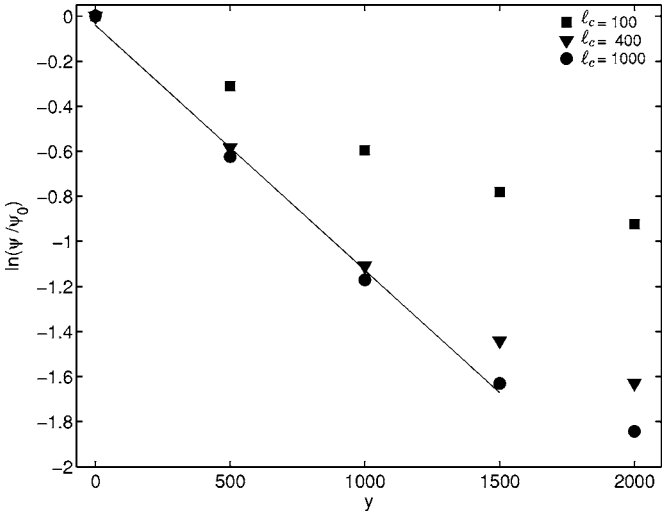

FIG. 12. Same as in Fig. 11, but in 2D isotropic media with a cutoff ℓ_c for the extent of the correlations, and $\rho=1.5$. For the largest ℓ_c the medium behaves essentially as a completely correlated system and, therefore, the amplitudes should decay exponentially. The straight line indicates that this is the case.

tion function for the local elastic constants $\lambda(\mathbf{x})$, with $\rho=1.2$ and 1.5. The wave amplitudes for the correlated cases decline very fast, much faster than those in the uniformly random medium. The results shown in Fig. 11 are consistent with the RG prediction that, acoustic waves in 2D systems must be localized for $\rho>\frac{1}{2}d=1$.

As is well-known, in the case of electron localization, the amplitudes $\psi(\mathbf{x})$ in *isotropic* media decay exponentially,

$$\psi(\mathbf{x}) = \psi_0 \exp(-|\mathbf{x}|/\xi). \tag{35}$$

However, it is not yet clear how ψ should decay in an *anisotropic medium* of the type that we have considered in the present paper. The question of how the wave's amplitude decays in such anisotropic media should presumably depend on whether the main direction of wave propagation is (more or less) parallel to the strata or perpendicular to them. Therefore, we rewrite Eq. (35) in a slightly more general form,

$$\psi(\mathbf{x}) = \psi_0 \exp[-(|\mathbf{x}|/\xi)^{\zeta}]. \tag{36}$$

If we fit the results for the 2D correlated media shown in Fig. 11 to Eq. (36) (which are for the case in which the main direction of wave propagation is parallel to the strata), we find that, $\zeta \simeq 1$ for both values of ρ. That is, one has the usual localization in which the wave's amplitude decays exponentially with the distance from the source.

The decay in the wave's amplitudes in an isotropic 2D medium with $\rho=1.5$, in which there is a cutoff length scale ℓ_c in the extent of the correlations, is shown in Fig. 12. The cutoff is measured in units of the distance between two nearest-neighbor grid points. When the cutoff is relatively short, the amplitude decay is slow, as the system behaves as a random one at large length scales. As the cutoff ℓ_c increases, the extent of the correlations between the grid blocks increases and, therefore, the medium's behavior approaches that of one in which the extent of the correlations is as large

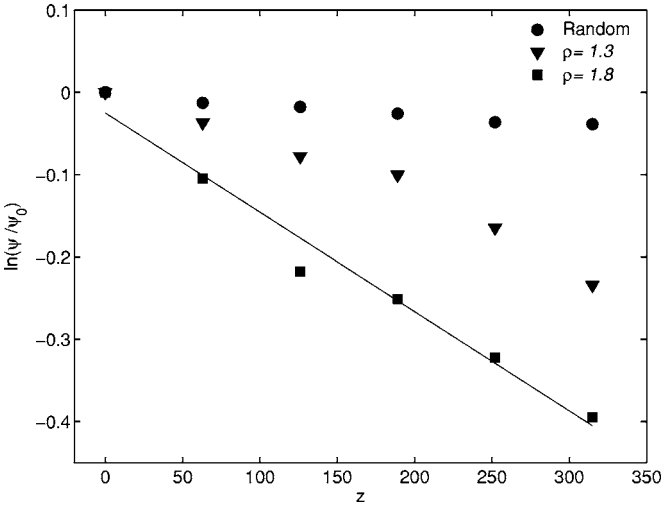

FIG. 13. Wave amplitudes in 3D isotropic media with negative ($\rho=1.3$) and positive ($\rho=1.8$) correlations, and their comparison with random media. The RG analysis indicates that for $\rho>1.5$ the waves must be localized and, therefore, their amplitudes must decay exponentially. The straight line indicates that this is the case.

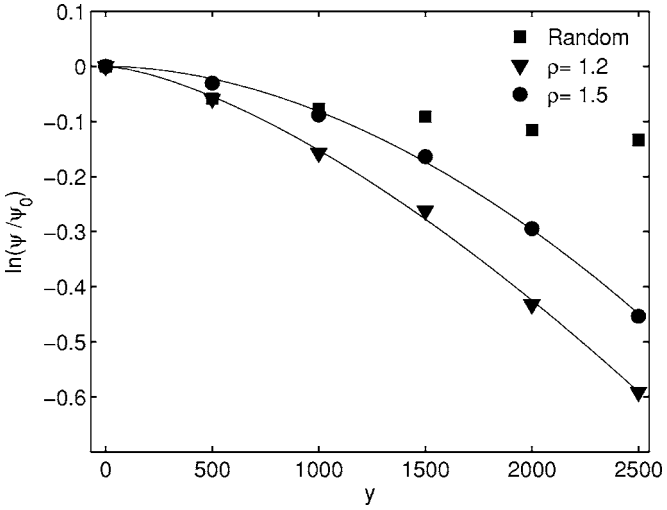

FIG. 14. Wave amplitudes in 2D anisotropic media in which the main direction of wave propagation is *perpendicular* to the strata. The curves indicate the best fits to the data.

as the system's size. For the largest cutoff length scale, $\ell_c=1000$, the medium essentially behaves like a completely correlated one.

Figure 13 presents the wave's amplitude decay in isotropic 3D systems for $\rho=1.3$ (negative correlations) and $\rho=1.8$ (positive correlations). Also shown are the results for a uniformly random 3D medium, but with the same variance as that of the correlated distribution of the local elastic constants. When the correlations are positive ($\rho=1.8$), the decay in the wave amplitudes is essentially exponential (indicated by the straight line), because there are zones of positively correlated (more or less similar) elastic constants that help to trap the wave front, hence resulting in the fast decay of the amplitudes. A fit of the numerical results for $\rho=1.8$ to Eq. (36) also confirms that, $\zeta\simeq 1$, consistent with the RG prediction that, in 3D, for $\rho>\frac{1}{2}d=3/2$ the waves must be localized. In contrast, the wave amplitudes in the random medium is practically constant, while in the medium with $\rho=1.3<3/2$ the amplitudes do not seem to decay fast enough. While the RG analysis does not predict localization of the waves in 3D systems with $\rho<1.5$, a fit of the results for $\rho=1.3$ shown in Fig. 13 indicates that, $\zeta\simeq 0.1$, although this estimate of ζ is not very accurate because the system is somewhat short.

In a practical application of propagation of acoustic waves in rock, such as seismic exploration, the main direction of wave propagation may more or less be *perpendicular* to the planes of the strata. For example, in seismic exploration the wave source is typically on the ground surface while the strata are more or less parallel to the ground surface, implying that the waves penetrate the ground and move perpendicular to the strata. Figure 14 presents the results of the numerical simulations for such a system in 2D. The decay in the wave's amplitudes appear to be fast. A fit of the results to Eq. (36) indicates that, $\zeta\simeq 1.4$. Figure 15 shows the corresponding results in 3D, indicating the same qualitative behavior. We have no plausible explanation at this point for this surprising result, which corresponds to *superlocalization* of the waves. We should, however, point out that we cannot rule out the possibility that, if we carry out much more extensive simulations with much larger systems, we would obtain the usual localization with $\zeta=1$. We are currently carrying out more extensive simulations which are, however, very time consuming.

We emphasize once again that our RG analysis, in its present form, does not make any prediction for the nature of wave localization in the type of anisotropic media that we study in this paper. Thus, whether Eq. (36) with $\zeta\neq 1$ represents a general result for the type of anisotropic media that we studied remains to be seen. However, as argued above, the possibility that $\zeta>1$ is very interesting, and deserves further study.

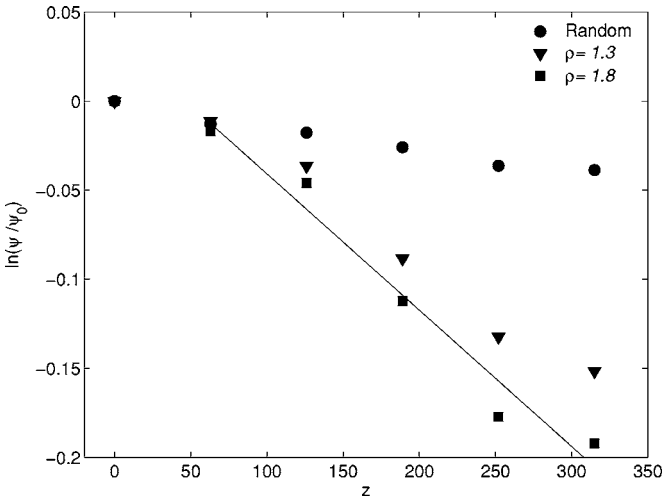

FIG. 15. Same as in Fig. 14, but for wave amplitudes in 3D anisotropic media in which the main direction of wave propagation is perpendicular to the strata.

V. SUMMARY

We showed that, depending on the nature of the disorder, acoustic waves in strongly disordered media can be localized or delocalized in *any* dimensions. In particular, they can be extended in disordered 1D systems if the correlation function for the distribution of the local elastic constants is of nondecaying power-law type, and that the waves are localized in *any* dimension if the exponent ρ of the power-law correlation function is larger than $\frac{1}{2}d$ (or, equivalently, the Hurst exponent H is larger than $\frac{1}{2}d-1$). These results, which contradict the generally accepted view that off-diagonal disorder has a much weaker effect on localization than the diagonal disorder, have important practical implications.

For example, as pointed out in the Introduction, in order for seismic records to contain meaningful information on the geology and content of a natural porous formation of linear size L, the localization length ξ must be larger L. Otherwise, propagation and scattering of such waves can provide information on the formation only up to length scale ξ; one cannot obtain meaningful information at larger length scales.[13] The localization length ξ is, clearly, a function of the system's dimensionality, the exponent ρ and amplitude D_ρ, and other relevant physical parameters of the system. The determination of ξ remains a major numerical task.

Separately, we showed recently[27] that power-law correlations of the type that we consider in this paper give rise to rough, self-affine wave fronts in the heterogeneous media that we studied here. The self-affinity of the WFs is characterized by a roughness exponent α, which is estimated[28] as follows. We compute the second-order front-front correlation function, defined by

$$C(r) = \langle [d(x) - d(x+r)]^2 \rangle, \tag{37}$$

where $d(x)$ is the position of the WF. For example, in 2D and at a given x $d(x)$ is the WF distance along the y direction, the main direction of wave propagation, from the first row at $y=0$ (see Fig. 10), and the averaging, for each value of r (also a point on the WF), is over all values of x. For a self-affine rough front, one must have (Ref. 28),

$$C(r) \sim r^{2\alpha}, \tag{38}$$

where α is the roughness exponent. We showed[27] that in all the cases one has, to within a few percent of H,

$$\alpha = H = \rho - 1. \tag{39}$$

That is, the WF roughness exponent—a *dynamical property* of the medium—is equal to the Hurst exponent—a *static property* of the medium that characterizes the spatial distribution of its local elastic moduli. This opens up the possibility of determining the Hurst exponent H (or, equivalently, the exponent ρ) in a laboratory experiment. This aspect of the problem will be studied in a future paper.

As mentioned in the Introduction, localization of seismic waves in heterogeneous rock also has important implications for the analysis of the seismic data that are generated by an earthquake.[29] If the waves are localized in the rock, and if a station that monitors the seismic activity of the rock is at a distance from the earthquake's hypocenter which is larger than the waves' localization length, then, the data collected by the station will not provide any useful information about the seismic activity prior to and during the earthquake. The results of a study of this issue will be reported in a future paper.

ACKNOWLEDGMENTS

We would like to thank J. Cardy and A. Esmailpour for useful comments and discussions. The work of S.M.V.A. was supported in part by the NIOC.

*Present address, Department of Physics, Lancaster University, Lancaster, United Kingdom
†Electronic address: moe@iran.usc.edu
‡Electronic address: rahimitabar@iust.ac.ir

[1] N. Bleistein, J. K. Cohen, and J. W. Stockwell, Jr., *Mathematics of Multidimensional Seismic Imaging, Migration, and Inversion* (Springer, New York, 2001).
[2] M. Sahimi, *Heterogeneous Materials II* (Springer, New York, 2003).
[3] P. M. Adler and J.-F. Thovert, *Fractures and Fracture Networks* (Kluwer Publishers, Amsterdam, 1999); M. Sahimi, *Flow and Transport in Porous Media and Fractured Rock* (Wiley-VCH, Berlin, 1995).
[4] M. Sahimi and S. E. Tajer, Phys. Rev. E **71**, 046301 (2005).
[5] P. Sheng, *Introduction to Wave Scattering, Localization and Mesoscopic Phenomena* (Academic, San Diego, 1995).
[6] P. W. Anderson, Phys. Rev. **109**, 1492 (1958); N. F. Mott and W. D. Twose, Adv. Phys. **10**, 107 (1961).
[7] E. Abrahams, P. W. Anderson, D. C. Licciardello, and T. V. Ramakrishnan, Phys. Rev. Lett. **42**, 673 (1979).
[8] F. Wegner, Z. Phys. B **25**, 327 (1976); **35**, 207 (1979); **36**, 209 (1980); Nucl. Phys. B **180**[FS2], 77 (1981).
[9] B. Kramer and A. MacKinnon, Rep. Prog. Phys. **56**, 1469 (1993).
[10] P. W. Anderson, Philos. Mag. B **52**, 505 (1985); P. Sheng and Z. Q. Zhang, Phys. Rev. Lett. **57**, 1879 (1986); K. Arya, Z. B. Su, and J. L. Birman, *ibid.* **57**, 2725 (1986); M. Kaveh, Philos. Mag. B **56**, 693 (1987); C. M. Soukoulis, E. N. Economou, G. S. Grest, and M. H. Cohen, Phys. Rev. Lett. **62**, 575 (1989); D. S. Wiersma, P. Bartolini, A. Lagendijk, and R. Righini, Nature (London) **390**, 671 (1997).
[11] For recent experimental observation of weak localization of seismic waves see, for example, E. Larose, L. Margerin, B. A. van Tiggelen, and M. Campillo, Phys. Rev. Lett. **93**, 048501 (2004).
[12] P. C. Martin, E. D. Siggia, and H. A. Rose, Phys. Rev. A **8**, 423 (1973).
[13] F. Shahbazi, A. Bahraminasab, S. M. Vaez Allaei, M. Sahimi, and M. R. Rahimi Tabar, Phys. Rev. Lett. **94**, 165505 (2005).
[14] S. M. Cohen, J. Machta, T. R. Kirkpatrick, and C. A. Condat, Phys. Rev. Lett. **58**, 785 (1987); M. Foret, E. Courtens, R. Vacher, and J. B. Suck, *ibid.* **77**, 3831 (1996); Z. Ye and A.

Alvarez, Phys. Status Solidi B **214**, 285 (1999); B. C. Gupta and Z. Ye, Phys. Rev. E **67**, 036606 (2003).

[15] B. Souillard, Physica A **157**, 3 (1989); D. Sornette and B. Souillard, Europhys. Lett. **13**, 7 (1990); T. Robin and B. Souillard, *ibid.* **21**, 273 (1993); Physica A **193**, 79 (1993).

[16] V. Baluni and J. Willemsen, Phys. Rev. A **31**, 3358 (1985).

[17] The older literature in this area was reviewed by D. Sornette, Acustica **67**, 199 (1989); **67**, 251 (1989); **68**, 15 (1989).

[18] S. He and J. D. Maynard, Phys. Rev. Lett. **57**, 3171 (1986); J. D. Maynard, Rev. Mod. Phys. **73**, 401 (2001).

[19] C. Hodges, J. Sound Vib. **82**, 411 (1982); E. Guazzelli, E. Guyon, and B. Souillard, J. Phys. (Paris), Lett. **44**, 837 (1983); M. P. Van Albada and A. Lagendijk, Phys. Rev. Lett. **55**, 2692 (1985); P. E. Wolf and G. Maret, *ibid.* **55**, 2696 (1985); Y. Kuga and A. Ishimaru, J. Opt. Soc. Am. A **8**, 831 (1986); M. Belzons, P. Devillard, F. Dunlop, E. Guazzelli, O. Parodi, and B. Souillard, Europhys. Lett. **4**, 909 (1987).

[20] A. Ishimaru, *Wave Propagation and Scattering in Random Media* (Oxford University Press, Oxford, England, 1997).

[21] H. Furstenberg, Trans. Am. Math. Soc. **108**, 377 (1963); see also, Y. N. Tutubalin, Theory Prob. Appl. (USSR) **10**, 19 (1965).

[22] P. Dean, Proc. Phys. Soc. London **84**, 727 (1964).

[23] H. Matsuda and K. Ishii, Suppl. Prog. Theor. Phys. **45**, 56 (1970); K. Ishii, *ibid.* **53**, 77 (1973).

[24] M. A. Dablain, Geophysics **51**, 54 (1986); G. Kneib and C. Kerner, *ibid.* **58**, 576 (1993).

[25] R. F. Voss, in *Fundamental Algorithms for Computer Graphics*, edited by R. A. Earnshaw, NATO Advanced Study Institute, Series E: Applied Science, Vol. 17 (Springer-Verlag, Heidelberg, 1985), p. 805.

[26] N.-N. Pang, Y.-K. Yu, and T. Halpin-Healy, Phys. Rev. E **52**, 3224 (1995); H. A. Makse, S. Havlin, M. Schwartz, and H. E. Stanley, *ibid.* **53**, 5445 (1996); H. Hamzehpour and M. Sahimi, *ibid.* **73**, 056121 (2006).

[27] S. M. Vaez Allaei and M. Sahimi, Phys. Rev. Lett. **96**, 075507 (2006).

[28] F. Family and T. Vicsek, J. Phys. A **18**, L75 (1985).

[29] M. R. Rahimi Tabar, M. Sahimi, F. Ghasemi, K. Kaviani, M. Allamehzadeh, J. Peinke, M. Mokhtari, M. Vesaghi, M. D. Niry, A. Bahraminasab, S. Tabatabai, S. Fayyazbakhsh, and M. Akbari, in *Modelling Critical and Catastrophic Phenomena in Geoscience*, edited by P. Bhattacharyya and B. K. Chakrabarti (Springer, Berlin, 2006).